

# Theoretical Discovery of a Superconducting Two-Dimensional Metal–Organic Framework

Xiaoming Zhang,<sup>†,‡,§</sup> Yinong Zhou,<sup>‡</sup> Bin Cui,<sup>†,‡</sup> Mingwen Zhao,<sup>\*,†</sup> and Feng Liu<sup>\*,‡,||</sup>

<sup>†</sup>School of Physics and State Key Laboratory of Crystal Materials, Shandong University, Jinan, Shandong 250100, China

<sup>‡</sup>Department of Materials Science and Engineering, University of Utah, Salt Lake City, Utah 84112, United States

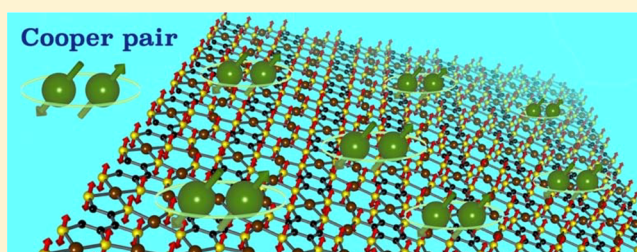
<sup>§</sup>Institute for Advanced Study, Tsinghua University, Beijing 100084, China

<sup>||</sup>Collaborative Innovation Center of Quantum Matter, Beijing 100084, China

## Supporting Information

**ABSTRACT:** Superconductivity is a fascinating quantum phenomenon characterized by zero electrical resistance and the Meissner effect. To date, several distinct families of superconductors (SCs) have been discovered. These include three-dimensional (3D) bulk SCs in both inorganic and organic materials as well as two-dimensional (2D) thin film SCs but only in *inorganic* materials. Here we predict superconductivity in 2D and 3D *organic* metal–organic frameworks by using first-principles calculations. We show that the highly conductive and recently synthesized Cu-benzenehexathial (BHT) is a Bardeen–Cooper–Schrieffer SC. Remarkably, the monolayer Cu-BHT has a critical temperature ( $T_c$ ) of 4.43 K, while  $T_c$  of bulk Cu-BHT is 1.58 K. Different from the enhanced  $T_c$  in 2D inorganic SCs which is induced by interfacial effects, the  $T_c$  enhancement in this 2D organic SC is revealed to be the out-of-plane soft-mode vibrations, analogous to surface mode enhancement originally proposed by Ginzburg. Our findings not only shed new light on better understanding 2D superconductivity but also open a new direction to search for SCs by interface engineering with organic materials.

**KEYWORDS:** Superconductivity, metal–organic framework, enhanced critical temperature, first-principles calculations



Since the first discovery of superconductor (SC) a century ago,<sup>1</sup> the field of superconductivity research has been continuously filled with exciting discoveries of new SCs. The first generation of SCs includes metal conductors, either elemental metal,<sup>1</sup> metal alloys,<sup>2</sup> or metallic phase of pressurized semiconductors.<sup>3</sup> They are conventional Bardeen–Cooper–Schrieffer (BCS) SCs<sup>4</sup> with a relatively low critical temperature ( $T_c$ ) determined by electron–phonon interaction. The second generation came as a breakthrough in the field with the discovery of high- $T_c$  copper oxides SCs.<sup>5,6</sup> The third-generation SCs is a family of Fe-based pnictide compounds.<sup>7</sup>

For all the three families of 3D bulk SCs, their 2D thin-film counterparts have also been actively pursued,<sup>8–10</sup> especially with the recent advance in epitaxial growth of thin films with single atomic layer precision. 2D SCs are appealing for fundamental study, with interesting properties pertaining to 2D geometry, and have potential applications for making 2D SC devices. It is expected that the superconductivity may interplay with other quantum effects at the 2D limit, such as charge localization,<sup>11</sup> quantum size effect,<sup>12</sup> spin-valley locking,<sup>13</sup> quantum metal,<sup>14,15</sup> and topological quantum phase transitions.<sup>16–18</sup> Recent studies have found some 2D SCs, such as  $\text{La}_{2-x}\text{Sr}_x\text{CuO}/\text{La}_2\text{CuO}_{4+\delta}$  interface<sup>19</sup> and FeSe single layer,<sup>20</sup> exhibit a  $T_c$  much higher than their 3D counterparts owing to interfacial phonon mode coupling<sup>21</sup> and electrical field effect.<sup>22</sup>

However, all of the known thin-film and 2D SCs are inorganic materials.<sup>8–10</sup>

Here, we predict for the first time superconductivity in both 2D and 3D organic metal–organic frameworks (MOFs). Using first-principles calculations, we show that single-atomic-layer Cu-benzenehexathial (Cu-BHT) is a BCS 2D SC with a  $T_c$  of 4.43 K, while the 3D Cu-BHT has a  $T_c$  of 1.58 K. We reveal that the enhanced  $T_c$  in the single layer Cu-BHT is caused by the out-of-plane soft-mode vibrations allowed at the 2D limit, consistent with the softening of surface modes to enhance  $T_c$  of thin-film SCs as envisioned by Ginzburg.<sup>23</sup> We emphasize that it is mechanistically different from interfacial effects as discovered in 2D inorganic SCs.<sup>21,22</sup>

Our study is largely motivated by the recent discovery of surprisingly high room-temperature electrical conductivity up to  $1580 \text{ s}\cdot\text{cm}^{-1}$  in Cu-BHT,<sup>24</sup> in contrast to conventional MOFs which are commonly insulating or semiconducting. In principle, any nonmagnetic metal could become superconducting at a sufficiently low temperature. This experimental observation intrigued us to investigate the possible superconductivity in Cu-BHT. Furthermore, because Cu-BHT has a

**Received:** July 2, 2017

**Revised:** September 11, 2017

**Published:** September 12, 2017

layered structure, we want to find out whether this unique material, with the highest conductivity among all the known MOFs to date,<sup>24</sup> will offer the first 2D organic SC.

**Computational Methods.** The calculations are performed using density-functional theory with generalized gradient approximation in the form of Perdew–Burke–Ernzerhof.<sup>25</sup> To eliminate the interlayer interaction, single-layer Cu-BHT is simulated by introducing a vacuum layer larger than 15 Å. The superconducting properties were calculated by QUANTUM ESPRESSO code<sup>26</sup> using the norm-conserving pseudopotentials with the cutoff energy of 100 Ry for the wave functions and the Brillouin zone (BZ) sampling of  $8 \times 8 \times 1$  ( $4 \times 4 \times 1$  for two- and three-layers Cu-BHT,  $4 \times 4 \times 8$  for bulk Cu-BHT) Monkhorst–Pack  $k$ -point grids with a Methfessel–Paxton smearing of 0.07 Ry. Using the above  $k$ -point samplings for self-consistent cycle, the dynamic matrixes are calculated on a  $4 \times 4 \times 1$  ( $2 \times 2 \times 1$  for two- and three-layers Cu-BHT,  $4 \times 4 \times 8$  for bulk Cu-BHT)  $q$ -point mesh. The van der Waals (vdW) interaction is considered in multilayer and bulk Cu-BHT. The electronic band structures, orbital contributions, and charge density isosurfaces were analyzed by Vienna ab initio simulation package<sup>27</sup> with the energy cutoff of 500 eV being used on a  $7 \times 7 \times 1$  ( $5 \times 5 \times 9$  for bulk Cu-BHT) Monkhorst–Pack sampling in BZ.

**Results and Discussion.** The atomic structure of single layer Cu-BHT is shown in Figure 1a. Copper atoms are bridged

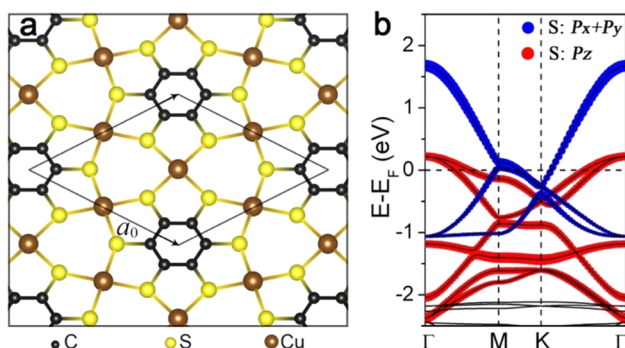


**Figure 1.** Crystal and band structure of single layer Cu-BHT. (a) Schematic of the crystal structure with the unit cell indicated by a rhombus.  $a_0$  is the lattice constant. (b) Band structure with the contributions of  $p_z$  and  $p_x + p_y$  orbitals of S atoms being indicated by red and blue disks, respectively.

by BHTs via Cu–S bonds, forming a perfect Kagome lattice with the point group of  $D_{6h}$ . The calculated equilibrium lattice constant  $a_0$  is 8.80 Å, in good agreement with the previous calculation (8.76 Å).<sup>24</sup> From the orbital-resolved band structures of Cu-BHT shown in Figure 1b (also see Figure S1a and Figure S1b in Supporting Information), one can clearly see the intrinsic metallic nature with multiple bands crossing the Fermi level. These bands are characterized with symmetry-guided coordination between  $S_{p_x+p_y}$  orbitals (Figure 1b) and  $Cu_{d_{xy}+d_{x^2-y^2}}$  orbitals (Figure S1b) and between  $S_{p_z}$  orbitals (Figure 1b),  $C_{p_z}$  orbitals (Figure S1a), and  $Cu_{d_{xz}+d_{yz}}$  orbitals (Figure S1b). Together they form a high density of 2D  $\pi$ - $d$  electron gas at the Fermi level, where the electronic density of states (DOS) reaches up to 3.56 states/eV/unit cell. The distribution of charge density difference ( $\Delta\rho$ ) with respect to isolated atoms is plotted in Figure S2, which clearly shows the formation of covalent bonds between Cu and S. Apparently,

such high DOS at Fermi level favors BCS-type superconductors.

The Fermi surface contour of single layer Cu-BHT is shown in Figure 2a, where one can see several hole/electron pockets in

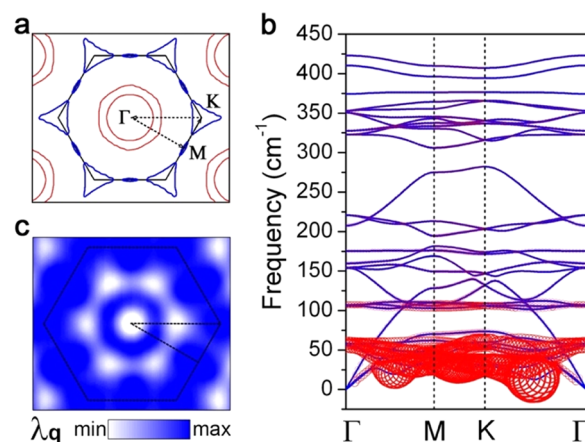


**Figure 2.** Fermi surface contour, phonon spectrum, and electron–phonon coupling of single layer Cu-BHT. (a) Fermi surface contour in the reciprocal space. (b) Phonon spectrum with the size of red circles being drawn proportional to the magnitude of EPC  $\lambda_{qv}$ . (c) The distribution of  $q$ -resolved electron–phonon coupling  $\lambda_q$ .

the BZ. The two hole pockets centered at a  $\Gamma$  point have the characteristics of  $\pi$ -bands stemming from the  $p_z$  orbitals of C and S atoms along with the  $d_{xz} + d_{yz}$  orbitals of Cu, which can be seen more clearly from the partial charge density shown in Figure S1c. An electron pocket at the K point and a hole pocket at the M point around the boundary of BZ have the  $\sigma$ -band characteristics arising from  $p_x + p_y$  orbitals of S and  $d_{xy} + d_{x^2-y^2}$  orbitals of Cu atoms, as shown in Figure S1d. Figure 2b shows the phonon dispersion  $\omega_{qv}$  with the frequency lower than 450  $\text{cm}^{-1}$ , which confirms the dynamic stability of 2D Cu-BHT by the absence of imaginary frequency modes. The phonon dispersion over whole frequency range and the projected phonon density of state (PhDOS) are displayed in Figure S3. Both Cu and S atoms dominate the vibration modes with frequencies below 450  $\text{cm}^{-1}$ . The interaction between C and S atoms contributes to the intermediate-frequency region between 450 and 1000  $\text{cm}^{-1}$ . The in-plane stretching modes of C atoms occupy the high frequencies above 1000  $\text{cm}^{-1}$ .

Figure 2b also shows the calculated electron–phonon coupling (EPC) strength  $\lambda_{qv}$  (red circles),

$$\lambda_{qv} = \frac{4}{\omega_{qv} N(0) N_k} \sum_{k,n,m} |g_{kn,k+qm}^v|^2 \delta(\epsilon_{kn}) \delta(\epsilon_{k+qm}) \quad (1)$$

$$g_{kn,k+qm}^v = \frac{\langle kn | \delta V / \delta u_{qv} | k + qm \rangle}{\sqrt{2\omega_{qv}}} \quad (2)$$

where  $N(0)$  and  $N_k$  are respectively the electron DOS and the number of  $k$  points at the Fermi level.  $u_{qv}$  is the amplitude of the displacement of phonon, and  $V$  is the Kohn–Sham potential.  $g_{kn,k+qm}^v$  is the scattering amplitude of an electronic state  $|k + qm\rangle$  into another state  $|kn\rangle$  resulting from the change in the self-consistent field potential  $\delta V / \delta u_{qv}$  arising from a phonon  $\omega_{qv}$ . The size of the red circles in Figure 2b is drawn proportional to the EPC  $\lambda_{qv}$  for the corresponding phonon mode. One can clearly see that the low-energy optical branches with the frequencies around 50  $\text{cm}^{-1}$  possess the strongest

electron–phonon couplings, while the contribution from other branches is negligible. Moreover, the softening of one acoustic branch yields significant coupling between electrons and acoustic phonons. Knowing the main phonon modes that couple with electron/hole pockets, one can reveal the distribution of electron–phonon couplings over the whole BZ and hence determine the contribution of the electron/hole pockets at the Fermi level. The momentum-dependent coupling  $\lambda_{\mathbf{q}}$ , as calculated by  $\lambda_{\mathbf{q}} = \sum_{\nu} \lambda_{\mathbf{q}\nu}$ , is plotted in Figure 2c. It reveals that the electron/hole pockets with  $\sigma$ -band characteristics at the boundary of BZ contribute predominantly to the EPC, while the hole pockets with the  $\pi$ -band characteristics centered at  $\Gamma$  point make relatively small contributions.

Next, we compare the Eliashberg function  $\alpha^2F(\omega)$ , the cumulative frequency-dependent EPC function  $\lambda(\omega)$ , and the displacement decomposed partial PhDOS to analyze the contributions of directional atomic vibration to the EPC constant.

$$\alpha^2F(\omega) = \frac{1}{2N_{\mathbf{q}}} \sum_{\mathbf{q}\nu} \lambda_{\mathbf{q}\nu} \omega_{\mathbf{q}\nu} \delta(\omega - \omega_{\mathbf{q}\nu}) \quad (3)$$

$$\lambda(\omega) = 2 \int_0^{\omega} \frac{\alpha^2F(\omega')}{\omega'} d\omega' \quad (4)$$

Figure 3 clearly indicates that the predominant contribution is from the out-of-plane vibrations of S atoms, which lead to a

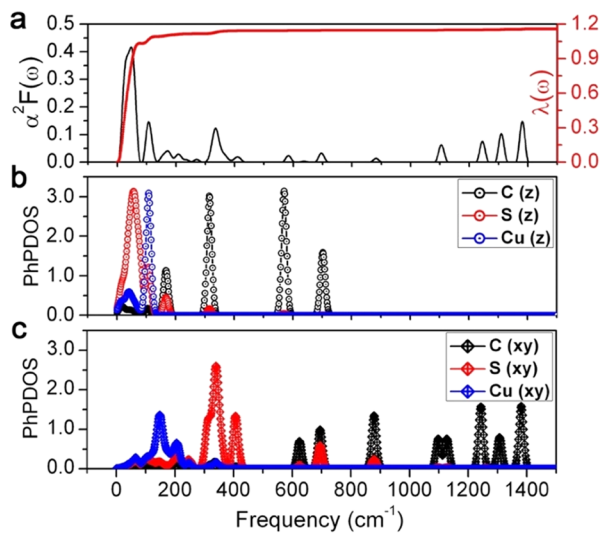


**Figure 3.** Eliashberg spectral function and partial PhDOS of single layer Cu-BHT. (a) Eliashberg spectral function  $\alpha^2F(\omega)$  and cumulative frequency-dependent  $\lambda(\omega)$ . (b, c) Partial PhDOS projected on (b) the out-of-plane ( $z$ , perpendicular to the Cu-BHT plane) and (c) the in-plane ( $xy$ , parallel to the Cu-BHT plane) vibrations of C, S, and Cu atoms.

sharp peak in  $\alpha^2F(\omega)$  at the frequencies around  $50 \text{ cm}^{-1}$ . Another contribution stems from the out-of-plane vibrations of Cu atoms, which result in a small increment of EPC at the narrow frequency range, around  $100 \text{ cm}^{-1}$ . Given the electronic states of S and Cu atoms at the Fermi level, the out-of-plane vibrations couple with the  $\sigma$ -band characteristic electron/hole pockets at the Fermi level, which is consistent with the distributions of  $\lambda_{\mathbf{q}}$  shown in Figure 2c. Even through symmetry allows the coupling between the  $\pi$ -band characteristic hole

pockets and in-plane optical stretching modes of carbon atoms, the high frequency (larger than  $1000 \text{ cm}^{-1}$ ) of such stretching mode makes it almost negligible, similar to graphene.<sup>28</sup> The total EPC is found to be  $\lambda = 1.16$  when  $\omega \rightarrow \infty$ , which makes the 2D single layer Cu-BHT an intermediate to strong conventional superconductor. This large value of  $\lambda$  is likely resulted from a very high density of states with multiple electron/hole packets forming time reversal pairs at the Fermi level (see Figure 2a) to facilitate a strong electron–phonon coupling (see Figure 2c).

Using the above values, the logarithmically averaged frequency defined as  $\langle \omega \rangle_{\log} = \exp\left[\frac{2}{\lambda} \int \frac{d\omega}{\omega} \alpha^2F(\omega) \log \omega\right]$  is calculated to be  $51.8 \text{ K}$  or  $35.96 \text{ cm}^{-1}$ . The  $T_c$  is estimated according to the Allen–Dynes<sup>29</sup> modified McMillan’s formula:<sup>30</sup>

$$T_c = \frac{\langle \omega \rangle_{\log}}{1.2} \exp\left[\frac{-1.04(1 + \lambda)}{\lambda - \mu^*(1 + 0.62\lambda)}\right] \quad (5)$$

where  $\mu^*$  is the retarded Coulomb potential. Using the typical value of  $\mu^* = 0.1$ , the above formula gives  $T_c = 4.43 \text{ K}$ .

It would be interesting to know whether bulk Cu-BHT is also a SC; if so, how is its  $T_c$  compared with a single layer Cu-BHT? The crystal structure of bulk Cu-BHT is presented in Figure S4, which shows a slight slippage between the neighboring two layers. From the comparison between the phonon dispersions of bulk and single layer Cu-BHT (Figure S5a), one significant impact caused by the bulk interlayer vdW interaction is hardening of the low-energy optical branches around  $50 \text{ cm}^{-1}$  in single layer Cu-BHT, which suppress the coupling between  $\sigma$ -band states and out-of-plane vibrations. Consequently, the intralayer EPC strength decreases to 0.10, smaller by 10% than the monolayer, as shown in Figure 4. Notably, Figure 4 also shows that the interlayer interaction enhances the EPC (approximately 0.41) along the  $\Gamma$ –Z direction, which is the direction contributing mainly to the EPC of bulk Cu-BHT. The underlying mechanism is similar to that in GIC,<sup>31,32</sup> where the interlayer states play the key roles in enhancing EPC, as evidenced by the abundant electron/hole pockets at the middle section of BZ (Figure S5b). Despite this, the overall EPC is significantly suppressed, leading to a drop of the first dominant peak in Eliashberg function  $\alpha^2F(\omega)$ , as shown in Figure 4b. The total EPC constant and the logarithmically averaged frequency for bulk Cu-BHT is 0.51 and  $122.7 \text{ K}$ , respectively, which give  $T_c = 1.58 \text{ K}$  as estimated by the McMillan–Allen–Dynes formula. In terms of electronic states, going from 2D to bulk Cu-BHT, both the breakage of  $\pi$ -band states in carbon rings and the weakening of S–Cu  $\sigma$ -band states at Fermi level (see the right panel of Figure S4) decrease the effective DOS  $N(0)$ , leading to fewer coupling modes available between electrons and phonons. This effect is similar to LiC<sub>6</sub> where the  $T_c$  of Li-intercalated graphite is lower than that of Li-intercalated graphene due to the reduction of electronic states of Li at the Fermi level.<sup>33</sup>

Additionally, the thickness dependence of  $T_c$  is an important property for 2D superconductors, as shown experimentally in amorphous Bi films,<sup>34</sup> ultrathin Pb films,<sup>35</sup> and NbSe<sub>2</sub> multilayers.<sup>36</sup> So we have further calculated EPC constant and  $T_c$  in two- and three-layer Cu-BHT films, using the optimized film atomic structures as shown in Figure S6a and c, respectively. These structures are notably different from the bulk-terminated-surface structures with larger atomic relaxation

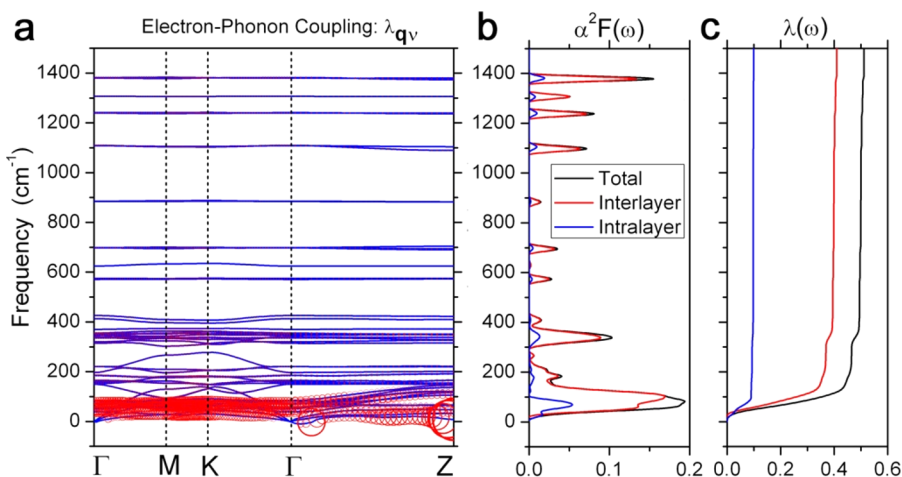


**Figure 4.** Superconducting properties of bulk Cu-BHT. (a) Phonon spectrum with the EPC  $\lambda_{q\nu}$  indicated by the red circles. (b) Eliashberg spectral function  $\alpha^2F(\omega)$  and (c) cumulative frequency-dependent  $\lambda(\omega)$ . The total (black line)  $\alpha^2F(\omega)$  and  $\lambda(\omega)$  are separated into interlayer (red line) and intralayer (blue line) contributions. The interlayer and intralayer EPC  $\lambda_{q\nu}$  for the corresponding phonon mode are plotted in Figure S5c and S5d, respectively.

changing the Cu–S bonds in different layers and decreasing the interlayer spacing. Consequently, the out-of-plane vibrations are significantly suppressed in two- and three-layer BHT films, and the electronic states at the Fermi level are modified to be rather different from those of single-layer film or bulk. The calculated EPC constant of the two- and three-layers Cu-BHT is 0.30 and 0.37 (Figure 5), which gives rise to a decreased  $T_c$  of

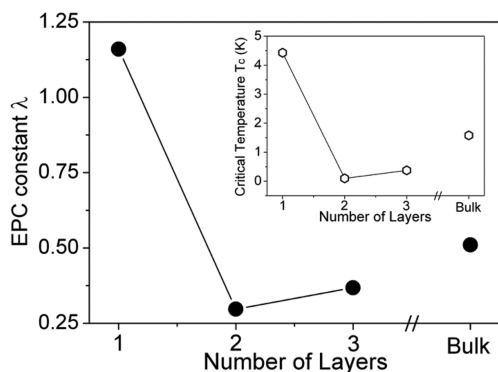


**Figure 5.** EPC constant  $\lambda$  and critical temperature  $T_c$  (inset) of optimized single-, two-, three-layer Cu-BHT film, and bulk Cu-BHT. The phonon spectrum, the  $\mathbf{q}$  and  $\nu$  resolved EPC  $\lambda_{q\nu}$ , the Eliashberg spectral function  $\alpha^2F(\omega)$ , and the cumulative frequency-dependent  $\lambda(\omega)$  of two- and three-layer Cu-BHT films are shown in Figure S6b and d, respectively.

$\sim 0.1$  and  $0.37$  K (inset of Figure 5), respectively. To better understand such a  $T_c$  reduction, we further did test calculations by using the unrelaxed two- and three-layer BHT films with the bulk-terminated-surface structures. Then the EPC constant is increased to 0.60 and 0.55 (Figure S7), which gives rise to a  $T_c$  of  $\sim 2.20$  and  $1.86$  K (inset of Figure S7), respectively. Note that both EPC constant and  $T_c$  would increase “monotonically” with the decreasing thickness (Figure S7) if the film would assume the bulk-terminated-surface structures, because then the out-of-plane vibrations and soft surface modes would enhance the EPC strength similar to the situation we discussed earlier for the single-layer Cu-BHT film.

We stress that the finding of bulk Cu-BHT being superconducting is a significant result in its own right, as it

represents the discovery of a new SC in organic materials of MOFs by theory. In fact, we expect that experimental confirmation of our theoretical prediction will likely come with bulk measurements first, since the metal-like high conductivity has already been observed at high temperature in the existing bulk samples,<sup>24</sup> and efforts are being made to prepare high-quality crystals and larger crystalline domains, as well as thin film and 2D samples.<sup>24</sup>

In conclusion, we envision that the study of superconductivity in Cu-BHT and related MOFs will potentially open a new avenue toward 2D and 3D organic SCs; given MOFs being one of biggest family of organic compounds, what we discovered here could be only a tip of the iceberg. Furthermore, our finding may also shed new light on better understanding the existing 2D inorganic SCs. We notice that similar 2D in-plane coordination of Cu–S, Cu–O, and Fe–Se bonding networks (Figure S8) exists in Cu-BHT, Cu–O plane in high  $T_c$  cuprate,<sup>6</sup> and single layer FeSe,<sup>20</sup> respectively, and they all play the key role in triggering the superconductivity in each system. Their Fermi surfaces are similar, having electron and/or hole pockets formed by d-orbitals of transition metals and p-orbitals of group-VI elements at high symmetry K points.  $T_c$  is expected to be strongly affected by doping, strain, thickness, and substrate (interface), which propose interesting subjects for future studies, especially considering the superconducting mechanisms in both cuprate and FeSe are still of high interest and under debatable. Last but not least, the discovery of superconductivity in a Kagome lattice is very interesting from the symmetry point view, as the Kagome lattice is the most intriguing playground for many exotic phenomena, such as fractional topological states<sup>37,38</sup> and quantum spin liquid phases.<sup>39,40</sup>

## ■ ASSOCIATED CONTENT

### Supporting Information

The Supporting Information is available free of charge on the ACS Publications website at DOI: 10.1021/acs.nanolett.7b02795.

Detailed electronic property and phonon spectrum of single layer Cu-BHT; details related to the superconducting properties of bulk Cu-BHT; thickness-

dependent superconducting property of Cu-BHT; in-plane coordination of Cu–O and Fe–Se bonding networks exist in high  $T_c$  cuprate and single layer FeSe (PDF)

## AUTHOR INFORMATION

### Corresponding Authors

\*E-mail: [fliu@eng.utah.edu](mailto:fliu@eng.utah.edu).

\*E-mail: [zmw@sdu.edu.cn](mailto:zmw@sdu.edu.cn).

### ORCID

Feng Liu: 0000-0002-3701-8058

### Notes

The authors declare no competing financial interest.

## ACKNOWLEDGMENTS

Y.Z. and F.L. acknowledge financial support from DOE-BES (no. DE-FG02-04ER46148). X.Z. and M.Z. acknowledge financial support from the National Natural Science Foundation of China (nos. 21433006, 11774201) and the National Key Research and Development Program of China (no. 2016YFA0301200). X.Z. and B.C. acknowledge support by the China Scholarship Council (no. 201506220046). We also thank Supercomputing Center at NERSC and CHPC at University of Utah for providing the computing resources.

## REFERENCES

- (1) Van Delft, D.; Kes, P. *Phys. Today* **2010**, 63, 38–43.
- (2) Hardy, G. F.; Hulm, J. K. *Phys. Rev.* **1954**, 93, 1004–1016.
- (3) Struzhkin, V. V.; Hemley, R. J.; Mao, H. K.; Timofeev, Y. A. *Nature* **1997**, 390, 382–384.
- (4) Bardeen, J.; Cooper, L. N.; Schrieffer, J. R. *Phys. Rev.* **1957**, 108, 1175–1204.
- (5) Bednorz, J. G.; Müller, K. A. Z. *Phys. B: Condens. Matter* **1986**, 64, 189–193.
- (6) Hor, P. H.; Gao, L.; Meng, R. L.; Huang, Z. J.; Wang, Y. Q.; Forster, K.; Vassiliou, J.; Chu, C. W.; Wu, M. K.; Ashburn, J. R.; Torng, C. J. *Phys. Rev. Lett.* **1987**, 58, 911–912.
- (7) Kamihara, Y.; Hiramatsu, H.; Hirano, M.; Kawamura, R.; Yanagi, H.; Kamiya, T.; Hosono, H. *J. Am. Chem. Soc.* **2006**, 128, 10012–10013.
- (8) Saito, Y.; Nojima, T.; Iwasa, Y. *Nat. Rev. Mater.* **2016**, 2, 16094.
- (9) Uchihashi, T. *Supercond. Sci. Technol.* **2017**, 30, 013002.
- (10) Brun, C.; Cren, T.; Roditchev, D. *Supercond. Sci. Technol.* **2017**, 30, 013003.
- (11) Mooij, J. E. *Two-dimensional transition in superconducting films and junction arrays*; Springer: Boston, 1984.
- (12) Guo, Y.; Zhang, Y. F.; Bao, X. Y.; Han, T. Z.; Tang, Z.; Zhang, L. X.; Zhu, W. G.; Wang, E. G.; Niu, Q.; Qiu, Z. Q.; Jia, J. F.; Zhao, Z. X.; Xue, Q. K. *Science* **2004**, 306, 1915–1917.
- (13) Saito, Y.; Nakamura, Y.; Bahramy, M. S.; Kohama, Y.; Ye, J.; Kasahara, Y.; Nakagawa, Y.; Onga, M.; Tokunaga, M.; Nojima, T.; Yanase, Y.; Iwasa, Y. *Nat. Phys.* **2015**, 12, 144–149.
- (14) Tsen, A. W.; Hunt, B.; Kim, Y. D.; Yuan, Z. J.; Jia, S.; Cava, R. J.; Hone, J.; Kim, P.; Dean, C. R.; Pasupathy, A. N. *Nat. Phys.* **2015**, 12, 208–212.
- (15) Saito, Y.; Kasahara, Y.; Ye, J.; Iwasa, Y.; Nojima, T. *Science* **2015**, 350, 409–413.
- (16) Wang, Z. F.; Zhang, H.; Liu, D.; Liu, C.; Tang, C.; Song, C.; Zhong, Y.; Peng, J.; Li, F.; Nie, C.; Wang, L.; Zhou, X. J.; Ma, X.; Xue, Q. K.; Liu, F. *Nat. Mater.* **2016**, 15, 968–973.
- (17) Berezinskii, V. L. *Sov. Phys. JETP* **1972**, 34, 610–616.
- (18) Kosterlitz, J. M.; Thouless, D. J. *J. Phys. C: Solid State Phys.* **1972**, 5 (11), L124–L126.
- (19) Gozar, A.; Logvenov, G.; Kourkoutis, L. F.; Bollinger, A. T.; Giannuzzi, L. A.; Müller, D. A.; Bozovic, I. *Nature* **2008**, 455, 782–785.
- (20) Wang, Q.-Y.; Li, Z.; Zhang, W.-H.; Zhang, Z.-C.; Zhang, J.-S.; Li, W.; Ding, H.; Ou, Y.-B.; Deng, P.; Chang, K.; Wen, J.; Song, C.-L.; He, K.; Jia, J.-F.; Ji, S.-H.; Wang, Y.-Y.; Wang, L.-L.; Chen, X.; Ma, X.-C.; Xue, Q.-K. *Chin. Phys. Lett.* **2012**, 29, 037402.
- (21) Lee, J. J.; Schmitt, F. T.; Moore, R. G.; Johnston, S.; Cui, Y. T.; Li, W.; Yi, M.; Liu, Z. K.; Hashimoto, M.; Zhang, Y.; Lu, D. H.; Devereaux, T. P.; Lee, D. H.; Shen, Z. X. *Nature* **2014**, 515, 245–248.
- (22) Shiohagi, J.; Ito, Y.; Mitsuhashi, T.; Nojima, T.; Tsukazaki, A. *Nat. Phys.* **2015**, 12, 42–46.
- (23) Ginzburg, V. L. *Phys. Lett.* **1964**, 13, 101–102.
- (24) Huang, X.; Sheng, P.; Tu, Z.; Zhang, F.; Wang, J.; Geng, H.; Zou, Y.; Di, C.-a.; Yi, Y.; Sun, Y.; Xu, W.; Zhu, D. *Nat. Commun.* **2015**, 6, 7408.
- (25) Perdew, J. P.; Burke, K.; Ernzerhof, M. *Phys. Rev. Lett.* **1996**, 77, 3865–3868.
- (26) Giannozzi, P.; Baroni, S.; Bonini, N.; Calandra, M.; Car, R.; Cavazzoni, C.; Ceresoli, D.; Chiarotti, G. L.; Cococcioni, M.; Dabo, I.; Dal Corso, A.; de Gironcoli, S.; Fabris, S.; Fratesi, G.; Gebauer, R.; Gerstmann, U.; Gougoussis, C.; Kokalj, A.; Lazzeri, M.; Martin-Samos, L.; Marzari, N.; Mauri, F.; Mazzarello, R.; Paolini, S.; Pasquarello, A.; Paulatto, L.; Sbraccia, C.; Scandolo, S.; Sclauzero, G.; Seitsonen, A. P.; Smogunov, A.; Umari, P.; Wentzcovitch, R. M. *J. Phys.: Condens. Matter* **2009**, 21, 395502.
- (27) Kresse, G.; Furthmüller, J. *Phys. Rev. B: Condens. Matter Mater. Phys.* **1996**, 54, 11169–11186.
- (28) Si, C.; Liu, Z.; Duan, W.; Liu, F. *Phys. Rev. Lett.* **2013**, 111, 196802.
- (29) Allen, P. B.; Dynes, R. C. *Phys. Rev. B* **1975**, 12, 905–922.
- (30) McMillan, W. L. *Phys. Rev.* **1968**, 167, 331.
- (31) Calandra, M.; Mauri, F. *Phys. Rev. Lett.* **2005**, 95, 237002.
- (32) Park, C.-H.; Giustino, F.; Cohen, M. L.; Louie, S. G. *Nano Lett.* **2008**, 8, 4229–4233.
- (33) Profeta, G.; Calandra, M.; Mauri, F. *Nat. Phys.* **2012**, 8, 131–134.
- (34) Liu, Y.; McGreer, K. A.; Nease, B.; Haviland, D. B.; Martinez, G.; Halley, J. W.; Goldman, A. M. *Phys. Rev. Lett.* **1991**, 67, 2068.
- (35) Qin, S.; Kim, J.; Niu, Q.; Shih, C.-K. *Science* **2009**, 324, 1314–1317.
- (36) Xi, X.; Zhao, L.; Wang, Z.; Berger, H.; Forró, L.; Shan, J.; Mak, K. F. *Nat. Nanotechnol.* **2015**, 10, 765–769.
- (37) Tang, E.; Mei, J.-W.; Wen, X.-G. *Phys. Rev. Lett.* **2011**, 106, 236802.
- (38) Liu, Z.; Wang, Z.-F.; Mei, J.-W.; Wu, Y.-S.; Liu, F. *Phys. Rev. Lett.* **2013**, 110, 106804.
- (39) Shores, M. P.; Nytko, E. A.; Bartlett, B. M.; Nocera, D. G. *J. Am. Chem. Soc.* **2005**, 127, 13462–13463.
- (40) Lee, P. A. *Science* **2008**, 321, 1306–1307.